Published in final edited form as:

Lipids. 2019 June ; 54(6-7): 411–418. doi:10.1002/lipd.12171.

Two specific sulfatide species are dysregulated during renal development in a mouse model of Alport Syndrome

Megan M. Gessel[1,*], **Jeffrey M. Spraggins**[4,5,6], **Paul Voziyan**[1,2], **Dale R. Abrahamson**[7], **Richard M. Caprioli**[3,4,5], **Billy Hudson**[1,2,3,5]

[1]Division of Nephrology, Vanderbilt University Medical Center, Nashville, TN 37232

[2]Center for Matrix Biology, Vanderbilt University Medical Center, Nashville, TN 37232

[3]Department of Medicine, Vanderbilt University Medical Center, Nashville, TN 37232

[4]Mass Spectrometry Research Center, Vanderbilt University Nashville, TN 37232

[5]Department of Biochemistry, Vanderbilt University Nashville, TN 37232

[6]Department of Chemistry, Vanderbilt University Nashville, TN 37232

[7]Department of Anatomy and Cell Biology, University of Kansas Medical Center, 3901 Rainbow Boulevard Kansas City, Kansas 66160[§§§].

Abstract

Alport syndrome is caused by mutations in collagen IV that alter the morphology of renal glomerular basement membrane. Mutations result in proteinuria, tubulointerstitial fibrosis, and renal failure but the pathogenic mechanisms are not fully understood. Using imaging mass spectrometry, we aimed to determine whether the spatial and/or temporal patterns of renal lipids are perturbed during the development of Alport syndrome in the mouse model.

Our results show that most sulfatides are present at similar levels in both the wild-type and the Alport kidneys, with the exception of two specific sulfatide species, SulfoHex-Cer(d18:2/24:0) and SulfoHex-Cer(d18:2/16:0). In the Alport but not in wild-type kidneys, the levels of these species mirror the previously described abnormal laminin expression in Alport syndrome. The presence of these sulfatides in renal tubules but not in glomeruli suggests that this specific aberrant lipid pattern may be related to the development of tubulointerstitial fibrosis in Alport disease.

Keywords

lipid; sulfatide; Alport syndrome; imaging mass spectrometry; basement membrane; kidney

To whom correspondence should be addressed: **Billy Hudson** Division of Nephrology and Hypertension, Department of Medicine, Vanderbilt University School of Medicine, D-3100 Medical Center North, Nashville, TN 37232, USA, Billy.hudson@vanderbilt.edu.

*Present address: Department of Chemistry, University of Puget Sound, 1500 N Warner Ave Tacoma, WA 98417

Conflict of Interest: No conflict of interest exists for any of the authors.

Introduction

Alport syndrome is an inherited disorder caused by mutations to the *COL4A3*, *COL4A4*, and *COL4A5* genes. It is marked by dysregulation of GBM proteins, including collagen IV and laminin, resulting in altered GBM morphology, proteinuria, and renal failure (Kashtan et al., 2001; Abrahamson et al., 2003; Hudson et al., 2003). Normally, laminin $\alpha_1\beta_1\gamma_1$ (LM-111) is expressed only during the early stages of glomerular development. In Alport syndrome, the LM-111 is re-expressed in the adult GBM (Abrahamson & St John 1993; Abrahamson et al., 2003; Abrahamson et al., 2007), although the mechanisms governing this re-expression are unclear. It has been shown that sulfatides, a class of acidic glycosphingolipids, can initiate basement membrane assembly by binding directly to LM-111 (Li et al., 2005). This finding suggested that sulfatides within the plasma membrane may play a role in laminin deposition. Given the dysregulation of laminin expression in the Alport GBM, we sought to determine if the renal sulfatide levels would follow an abnormal temporal pattern in Alport syndrome.

Sulfatides (3-O-sulfogalactosylceramides) consist of a ceramide with a sulfated galactose head group. Sulfatides have been found in a variety of tissues, including kidney, and have various structures, often depending on tissue type (Kyogashima et al., 2006). Changes in the sulfatide structure may influence its presentation at the cell surface and the degree of clustering of receptor molecules (Pruett et al., 2008). Alterations in sulfatide metabolism have been suggested to play a role in a number of diseases, including renal cell carcinoma, hepatorenal fibrocystic disease, and protein overload nephropathy (Li et al., 2009; Zhang et al., 2009; Takahashi & Suzuki 2012).

To investigate sulfatides in the intact renal tissue during kidney development, we used Matrix Assisted Laser Desorption Ionization Imaging Mass Spectrometry (MALDI IMS) (Caprioli et al., 1997). This technology combines the high sensitivity and selectivity of mass spectrometry with the spatial analysis provided by traditional histology, offering visualization of the distribution of specific biomolecules in tissue (McDonnell & Heeren 2007; Norris & Caprioli 2013; Gessel et al., 2014). This technology has been previously applied to the studies of lipids in renal diseases (Herring et al., 2007; Murphy et al., 2009; Kaneko et al., 2011; Marsching et al., 2011; Ruh et al., 2013; Grove et al., 2014; Jones et al., 2014).

We compared the temporal and spatial distribution of sulfatides in renal sections from the wild-type (WT) mice and a mouse model of Alport syndrome. The levels of two sulfatides, SulfoHex-Cer(d18:2/24:0) and SulfoHex-Cer(d18:2/16:0), dramatically increased in the Alport compared to WT kidneys during development up to 28 days of age. These temporal changes mirrored the known abnormality of laminin assembly in Alport syndrome. The sulfatide species were localized to renal tubules, thus suggesting that this aberrant lipid pattern may be related to the development of tubulointerstitial fibrosis in Alport disease. To the best of our knowledge, this is the first report suggesting a role for specific lipid species in the pathogenesis of Alport syndrome.

Methods

Animals.

Mice containing a target deletion of the NC1 domain of the α3(IV) collagen chain were obtained from Jackson Laboratory (mouse strain Jax 129-*Col4a3*^{tm1Dec} (Cosgrove et al., 1996)). The colony was maintained by heterozygote interbreeding and progeny were genotyped by polymerase chain reaction. Heterozygous and WT littermates served as controls. Left and right kidneys from 3 mice from each group at each age were analyzed. The study was approved by KUMC IACUC, protocol #2017–2389.

Materials.

1,5-Diaminonaphthalene (DAN) was purchased from Sigma-Aldrich (Milwaukee, WI). Conductive indium tin oxide (ITO)-coated microscope glass slides (2.5 × 6 cm) were purchased from Delta Technologies (Stillwater, MN). The sublimation apparatus was from Chemglass Life Sciences.

Sample preparation.

Whole kidneys were snap frozen and sectioned at 12 μm and thaw mounted onto ITO slides. Matrix was applied to the tissue by sublimation (Hankin et al., 2007). Approximately 300 mg of DAN was used (~0.16 mg/mm^2) and sublimated at 104°C and 50 mtorr for approximately 5 minutes. DAN has been shown to be an effective MALDI matrix for lipids (Dong et al., 2013). Sample slides were weighed before and after sublimation to ensure consistence between slides. Additionally, sections from each group were included on the same slide, in order to maintain matrix homogeneity between samples.

Mass Spectrometry.

Samples were analyzed on a 9.4T FT-ICR MS (Bruker Daltonics SolariX) in a negative ion mode. For FT-ICR experiments, data was acquired using ftmsControl software. Two hundred shots per spot were acquired with a 2 kHz repetition rate Smartbeam II Nd:YAG laser using the beam diameter setting of ~10 μm and a step size of 40 μm for low-resolution and 15 μm for high resolution images. An *m/z* range of 500 −1000 *m/z* was measured. Imaging data was visualized using FlexImaging 3.0 (Bruker Daltonics). Following MALDI IMS analysis and matrix removal, samples were stained with periodic acid Schiff (PAS) stain (Deutskens et al., 2011). MALDI MS/MS was performed using a MALDI-LTQ-XL hybrid linear ion trap instrument (ThermoScientific) using pulsed-q-dissociation.

Data Analysis.

Heat-map images were generated using FlexImaging software (Bruker Daltonics) for the entire tissue section to assess whether sulfatide levels were changing. To localize the signals to specific histological features of the tissue, the MALDI IMS images were overlayed with the scanned optical images using FlexImaging (Deutskens et al., 2011). Briefly, the scanned optical images of the PAS-stained slides were overlayed onto the IMS images in order to identify glomeruli and tubules in the tissue and correlate them to the IMS images. Regions of the image that corresponded to tubules were selected to generate average mass spectra for

tubules only. Average mass spectra from tubules from each group (2 day, 14 day and 28 day) were compared in order to evaluate differences in signal intensity and to generate a list of the masses of ions detected in the tissue. With the exact masses from the FTICR MALDI IMS experiment, the LIPID MAPS data base was used to identify the detected species, based on their detected masses. Spectra from the linear ion trap instrument were analyzed using Xcalibur (Thermo Fisher Scientific) and analysis of MS/MS daughter ions to identify the ions was performed manually.

Results

Multiple sulfatide lipids were detected and most showed the same levels in WT and Alport mice at 2, 14 and 28 days of age (Table S1). However, we identified two signals at *m/z* 888.6210 and 776.5005 with abundances that were similar in both groups at 2 and 14 days but dramatically increased at 28 days in Alport but not in WT mice (Fig. 1, Fig. S1). The signal was co-localized in the renal cortex (Fig 1, Fig S1). Other lipids were also detected in the sample (see Table S1 for a list of these species), but their overall levels did not appear to change (data not shown).

A database search (http://lipidmaps.org/) for *m/z* 888.6210 (3 ppm error) indicated that the mass corresponded to three potential lipid structures. These included three sulfatides with varying chain lengths and saturations: (d16:1/26:1), (d18:1, 24:1), and (d18:2, 24:0). To identify which compound was present in our tissue samples, MALDI MS/MS experiments were performed directly from the tissue surface (Fig. 2). Several sulfatide-specific fragments were present in the spectrum including peaks at *m/z* 97 and 241 (Hsu & Turk 2004). In addition, peaks specific to a doubly unsaturated sphingoid base (18:2) were present including *m/z* 538, 520, and 392 identifying the molecule at as SulfoHex-Cer(d18:2/24:0) (Fig. 2 A). Similar analysis of the peak at *m/z* 776.5005 identified this signal as SulfoHex-Cer(d18:2/16:0) (Fig. 2 B). Importantly, the high resolution experiments allowed us to exclude peaks at *m/z* 888.5561 and *m/z* 888.5709 that were nominally isobaric with the C^{13} isotopes of phospholipids. These phospholipid species did not change in WT vs. Alport kidneys and had very different tissue localizations compared to sulfatide species of interest (Fig. 3).

To determine specific localization of the two sulfatides of interest within the kidney, MALDI IMS data was acquired at 15 μm resolution. Following IMS analysis, the MALDI matrix was removed, the tissue stained with PAS and IMS images correlated with histological tissue features. The signal of SulfoHex-Cer(d18:2/24:0) (*m/z* 888.6224, 1.8 ppm error) was localized to tubular regions of the kidney but not to glomeruli (Fig. 4, Fig. S3). The tubular localization was the same in 2-day and 28-day old mice (data not shown). It was not possible to distinguish between proximal and distal tubules, due to the thickness of the section and the damage from the MALDI IMS laser.

Discussion

We have identified two renal tubular sulfatide species, SulfoHex-Cer(d18:2/24:0) and SulfoHex-Cer(d18:2/16:0), as potential players at the very early stages of tubulointerstitial

pathology in Alport syndrome. No other sulfatides with a diene sphingoid base were detected in this experiment, although it is possible that others do exist at concentrations below the sensitivity of MALDI IMS. The primary structural difference between these dysregulated sulfatide species and those sulfatides which levels were not affected in Alport is the presence of a second double bond in the sphingoid base of the dysregulated sulfatides. Sulfatides with a 4*E,* 14*Z*-diene in the sphingoid base of the ceramide moiety have been previously detected in mouse and human tissues (Panganamala et al., 1969; Renkonen & Hirvisalo 1969; Marsching et al., 2011).,

MALDI IMS is less sensitive than LC MS/MS, due to the small amount of analyte ions desorbed in one ablated spot and due to ion suppression from the heterogenous biomolecules that exist in the sampled tissue area. However, it does provide information about analyte tissue localization, which is key in this study. Another limitation of MALDI IMS is that absolute quantitative analysis is a significant challenge, again due to ion suppression affects, uneven tissue morphology which affects ionization, and challenges associated with standardization of analyte signal from tissue sections

In this study, the signal intensities of SulfoHex-Cer(d18:2/24:0) and SulfoHex-Cer(d18:2/16:0) were clearly different in WT and Alport mice at 28 days. This is apparent in both the heat map image shown in Figure 1 and in the extracted mass spectrum which is an average of all mass spectra collected from tubular regions (Figure S1). Other lipids, including sulfatides were detected in the MALDI IMS experiments (Table S1) and their signal intensities were not clearly different in Alport vs. WT kidneys (data not shown). Overall, our data support the conclusion that the expression of these specific sulfatide species is clearly altered between the groups.

Changes to sphingoid base saturation can confer bioactive properties to related lipid species. For example, sphingadienes, which are precursors of SulfoHex-Cer(d18:2/24:0) and SulfoHex-Cer(d18:2/16:0), have been shown to inhibit Akt-dependent and Wnt signaling in colon cancer cells (Fyrst et al., 2009; Kumar et al., 2012). In both cases, sphingosines containing single double bond did not show inhibitory effect. In another study, ceramides with an additional trans-double bond in the sphingoid backbone induced apoptosis in breast cancer cells (Struckhoff et al., 2004). In the current study, the diene sphingoid base was present only in the two sulfatide species that were dysregulated in Alport mice and not in any other identified sulfatide species. Overall, our results suggest that the second double bond is required for dysregulation of sulfatide levels in Alport mice.

Interestingly, the increase in renal levels of SulfoHex-Cer(d18:2/24:0) and SulfoHex-Cer(d18:2/16:0) at 28 days is similar to re-expression of LM-111 in the glomerular and tubular BM of Alport mice (Abrahamson & St John 1993; Abrahamson et al., 2003; Abrahamson et al., 2007), pointing to a potential relationship between these two phenomena. Although laminin expression was not measured in this study, the localization of SulfoHex-Cer(d18:2/24:0) and SulfoHex-Cer(d18:2/16:0) tubules would suggest that these sulfatides would interact with tubular rather than glomerular LM-111 as they specifically localize to the tubular regions of the kidney.

Although Alport disease is initiated in the glomerulus, later stages are characterized by progressive tubulointerstitial fibrosis in Alport mouse and in human kidneys (Kashtan & Kim 1992; Miner & Sanes 1996). Notably, tubulointerstitial fibrosis was observed in 79-day old Alport mice, while kidneys of 36-day old mice showed no clear signs of renal injury (Miner & Sanes 1996). Our detection of sulfatide dysregulation at 28 days, prior to appearance of histopathological lesions, suggests that these changes may be involved in very early stages of tubular injury. Because of the thickness of the tissue section and the damage from the MALDI laser, it was not possible to gain a more detailed view of the tissue histology from the sections that were imaged by MALDI IMS (e.g. localizing the signals to proximal vs. distal tubules or measuring the extend of tubular injury).

We speculate that one of the potential mechanisms of tubular injury involving sulfatides may be tubular reabsorption of profibrotic chemokines and cytokines secreted by stressed Alport podocytes, although this is not proven here (Ninichuk et al., 2005; Kruegel et al., 2013). Besides directly binding several chemokines, sulfatides can specifically affect monocyte infiltration into renal interstitium and trigger up-regulation of the chemokine co-receptor CXCR4 on leukocytes (Ogawa et al., 2004; Duchesneau et al., 2007; Takahashi & Suzuki 2012). Sulfatides can also bind to receptors on macrophages, thus triggering production of TGF-β1, a key cytokine in the pathogenesis of renal fibrosis (Popovic et al., 2007).

Supplementary Material

Refer to Web version on PubMed Central for supplementary material.

Acknowledgements:

This work was supported by grants from the National Institutes of Health 1F32DK097875 (to MMG); 5P41GM103391, 5R01GM058008 and 1S10OD012359 (to RMC); R01 DK065138 (to BGH and PAV); R01DK018381 (to BGH) and R24 DK103067 (to BGH, in part). The authors would like to acknowledge the Vanderbilt Shared Pathology resource for PAS stains of kidney tissue.

Abbreviations

BM	basement membrane
FT-ICR MS	Fourier transform ion cyclotron radiation mass spectrometry
GalCer	galactosylceramide
GBM	glomerular basement membrane
IMS	imaging mass spectrometry
LC	liquid chromatography
LM	Laminin
MALDI	Matrix assisted laser desorption ionization

References

Abrahamson DR, Isom K, Roach E, Stroganova L, Zelenchuk A, Miner JH & St John PL (2007). Laminin compensation in collagen alpha3(IV) knockout (Alport) glomeruli contributes to permeability defects. J Am Soc Nephrol, 18: 2465–2472. [PubMed: 17699809]

Abrahamson DR, Prettyman AC, Robert B & St John PL (2003). Laminin-1 reexpression in Alport mouse glomerular basement membranes. Kidney Int, 63: 826–834. [PubMed: 12631063]

Abrahamson DR & St John PL (1993). Laminin distribution in developing glomerular basement membranes. Kidney Int, 43: 73–78. [PubMed: 8433573]

Caprioli RM, Farmer TB & Gile J (1997). Molecular imaging of biological samples: localization of peptides and proteins using MALDI-TOF MS. Anal Chem, 69: 4751–4760. [PubMed: 9406525]

Cosgrove D, Meehan DT, Grunkemeyer JA, Kornak JM, Sayers R, Hunter WJ & Samuelson GC (1996). Collagen COL4A3 knockout: a mouse model for autosomal Alport syndrome. Genes Dev, 10: 2981–2992. [PubMed: 8956999]

Deutskens F, Yang JH & Caprioli RM (2011). High spatial resolution imaging mass spectrometry and classical histology on a single tissue section. Journal of Mass Spectrometry, 46: 568–571. [PubMed: 21630385]

Dong W, Shen Q, Baibado JT, Liang YM, Wang P, Huang YQ, Zhang ZF, Wang YX & Cheung HY (2013). Phospholipid analyses by MALDI-TOF/TOF mass spectrometry using 1,5-diaminonaphthalene as matrix. International Journal of Mass Spectrometry, 343: 15–22.

Duchesneau P, Gallagher E, Walcheck B & Waddell TK (2007). Up-regulation of leukocyte CXCR4 expression by sulfatide: an L-selectin-dependent pathway on CD4+ T cells. Eur J Immunol, 37: 2949–2960. [PubMed: 17853408]

Fyrst H, Oskouian B, Bandhuvula P, Gong Y, Byun HS, Bittman R, Lee AR & Saba JD (2009). Natural sphingadienes inhibit Akt-dependent signaling and prevent intestinal tumorigenesis. Cancer Res, 69: 9457–9464. [PubMed: 19934323]

Gessel MM, Norris JL & Caprioli RM (2014). MALDI imaging mass spectrometry: spatial molecular analysis to enable a new age of discovery. J Proteomics, 107: 71–82. [PubMed: 24686089]

Grove KJ, Voziyan PA, Spraggins JM, Wang S, Paueksakon P, Harris RC, Hudson BG & Caprioli RM (2014). Diabetic nephropathy induces alterations in the glomerular and tubule lipid profiles. J Lipid Res, 55: 1375–1385. [PubMed: 24864273]

Hankin JA, Barkley RM & Murphy RC (2007). Sublimation as a method of matrix application for mass spectrometric imaging. J Am Soc Mass Spectrom, 18: 1646–1652. [PubMed: 17659880]

Herring KD, Oppenheimer SR & Caprioli RM (2007). Direct tissue analysis by matrix-assisted laser desorption ionization mass spectrometry: application to kidney biology. Semin Nephrol, 27: 597–608. [PubMed: 18061842]

Hsu FF & Turk J (2004). Studies on sulfatides by quadrupole ion-trap mass spectrometry with electrospray ionization: structural characterization and the fragmentation processes that include an unusual internal galactose residue loss and the classical charge-remote fragmentation. J Am Soc Mass Spectrom, 15: 536–546. [PubMed: 15047058]

Hudson BG, Tryggvason K, Sundaramoorthy M & Neilson EG (2003). Alport's syndrome, Goodpasture's syndrome, and type IV collagen. N Engl J Med, 348: 2543–2556. [PubMed: 12815141]

Jones EE, Powers TW, Neely BA, Cazares LH, Troyer DA, Parker AS & Drake RR (2014). MALDI imaging mass spectrometry profiling of proteins and lipids in clear cell renal cell carcinoma. Proteomics, 14: 924–935. [PubMed: 24497498]

Kaneko Y, Obata Y, Nishino T, Kakeya H, Miyazaki Y, Hayasaka T, Setou M, Furusu A & Kohno S (2011). Imaging mass spectrometry analysis reveals an altered lipid distribution pattern in the tubular areas of hyper-IgA murine kidneys. Exp Mol Pathol, 91: 614–621. [PubMed: 21798258]

Kashtan CE & Kim Y (1992). Distribution of the alpha 1 and alpha 2 chains of collagen IV and of collagens V and VI in Alport syndrome. Kidney Int, 42: 115–126. [PubMed: 1635341]

Kashtan CE, Kim Y, Lees GE, Thorner PS, Virtanen I & Miner JH (2001). Abnormal glomerular basement membrane laminins in murine, canine, and human Alport syndrome: aberrant laminin alpha2 deposition is species independent. J Am Soc Nephrol, 12: 252–260. [PubMed: 11158215]

Kruegel J, Rubel D & Gross O (2013). Alport syndrome--insights from basic and clinical research. Nat Rev Nephrol, 9: 170–178. [PubMed: 23165304]

Kumar A, Pandurangan AK, Lu F, Fyrst H, Zhang M, Byun HS, Bittman R & Saba JD (2012). Chemopreventive sphingadienes downregulate Wnt signaling via a PP2A/Akt/GSK3beta pathway in colon cancer. Carcinogenesis, 33: 1726–1735. [PubMed: 22581840]

Kyogashima M, Tamiya-Koizumi K, Ehara T, Li G, Hu R, Hara A, Aoyama T & Kannagi R (2006). Rapid demonstration of diversity of sulfatide molecular species from biological materials by MALDI-TOF MS. Glycobiology, 16: 719–728. [PubMed: 16670104]

Li G, Hu R, Kamijo Y, Nakajima T, Aoyama T, Ehara T, Shigematsu H, Kannagi R, Kyogashima M & Hara A (2009). Kidney dysfunction induced by protein overload nephropathy reduces serum sulfatide levels in mice. Nephrology (Carlton), 14: 658–662. [PubMed: 19796024]

Li S, Liquari P, McKee KK, Harrison D, Patel R, Lee S & Yurchenco PD (2005). Laminin-sulfatide binding initiates basement membrane assembly and enables receptor signaling in Schwann cells and fibroblasts. J Cell Biol, 169: 179–189. [PubMed: 15824137]

Marsching C, Eckhardt M, Grone HJ, Sandhoff R & Hopf C (2011). Imaging of complex sulfatides SM3 and SB1a in mouse kidney using MALDI-TOF/TOF mass spectrometry. Anal Bioanal Chem, 401: 53–64. [PubMed: 21359825]

McDonnell LA & Heeren RM (2007). Imaging mass spectrometry. Mass Spectrom Rev, 26: 606–643. [PubMed: 17471576]

Miner JH & Sanes JR (1996). Molecular and functional defects in kidneys of mice lacking collagen alpha 3(IV): implications for Alport syndrome. J Cell Biol, 135: 1403–1413. [PubMed: 8947561]

Murphy RC, Hankin JA & Barkley RM (2009). Imaging of lipid species by MALDI mass spectrometry. J Lipid Res, 50 Suppl: S317–322. [PubMed: 19050313]

Ninichuk V, Gross O, Reichel C, Khandoga A, Pawar RD, Ciubar R, Segerer S, Belemezova E, Radomska E, Luckow B, Perez de Lema G, Murphy PM, Gao JL, Henger A, Kretzler M, Horuk R, Weber M, Krombach F, Schlondorff D & Anders HJ (2005). Delayed chemokine receptor 1 blockade prolongs survival in collagen 4A3-deficient mice with Alport disease. J Am Soc Nephrol, 16: 977–985. [PubMed: 15716328]

Norris JL & Caprioli RM (2013). Imaging mass spectrometry: a new tool for pathology in a molecular age. Proteomics Clin Appl, 7: 733–738. [PubMed: 24178781]

Ogawa D, Shikata K, Honke K, Sato S, Matsuda M, Nagase R, Tone A, Okada S, Usui H, Wada J, Miyasaka M, Kawashima H, Suzuki Y, Suzuki T, Taniguchi N, Hirahara Y, Tadano-Aritomi K, Ishizuka I, Tedder TF & Makino H (2004). Cerebroside sulfotransferase deficiency ameliorates L-selectin-dependent monocyte infiltration in the kidney after ureteral obstruction. J Biol Chem, 279: 2085–2090. [PubMed: 14583626]

Panganamala RV, Geer JC & Cornwell DG (1969). Long-chain bases in the sphingolipids of atherosclerotic human aorta. J Lipid Res, 10: 445–455. [PubMed: 4307832]

Popovic ZV, Sandhoff R, Sijmonsma TP, Kaden S, Jennemann R, Kiss E, Tone E, Autschbach F, Platt N, Malle E & Grone HJ (2007). Sulfated glycosphingolipid as mediator of phagocytosis: SM4s enhances apoptotic cell clearance and modulates macrophage activity. J Immunol, 179: 6770–6782. [PubMed: 17982067]

Pruett ST, Bushnev A, Hagedorn K, Adiga M, Haynes CA, Sullards MC, Liotta DC & Merrill AH Jr. (2008). Biodiversity of sphingoid bases (“sphingosines”) and related amino alcohols. J Lipid Res, 49: 1621–1639. [PubMed: 18499644]

Renkonen O & Hirvisalo EL (1969). Structure of plasma sphingadienine. J Lipid Res, 10: 687–693. [PubMed: 5356753]

Ruh H, Salonikios T, Fuchser J, Schwartz M, Sticht C, Hochheim C, Wirnitzer B, Gretz N & Hopf C (2013). MALDI imaging MS reveals candidate lipid markers of polycystic kidney disease. J Lipid Res, 54: 2785–2794. [PubMed: 23852700]

Struckhoff AP, Bittman R, Burow ME, Clejan S, Elliott S, Hammond T, Tang Y & Beckman BS (2004). Novel ceramide analogs as potential chemotherapeutic agents in breast cancer. J Pharmacol Exp Ther, 309: 523–532. [PubMed: 14742741]

Takahashi T & Suzuki T (2012). Role of sulfatide in normal and pathological cells and tissues. J Lipid Res, 53: 1437–1450. [PubMed: 22619219]

Zhang X, Nakajima T, Kamijo Y, Li G, Hu R, Kannagi R, Kyogashima M, Aoyama T & Hara A (2009). Acute kidney injury induced by protein-overload nephropathy down-regulates gene expression of hepatic cerebroside sulfotransferase in mice, resulting in reduction of liver and serum sulfatides. Biochem Biophys Res Commun, 390: 1382–1388. [PubMed: 19895791]

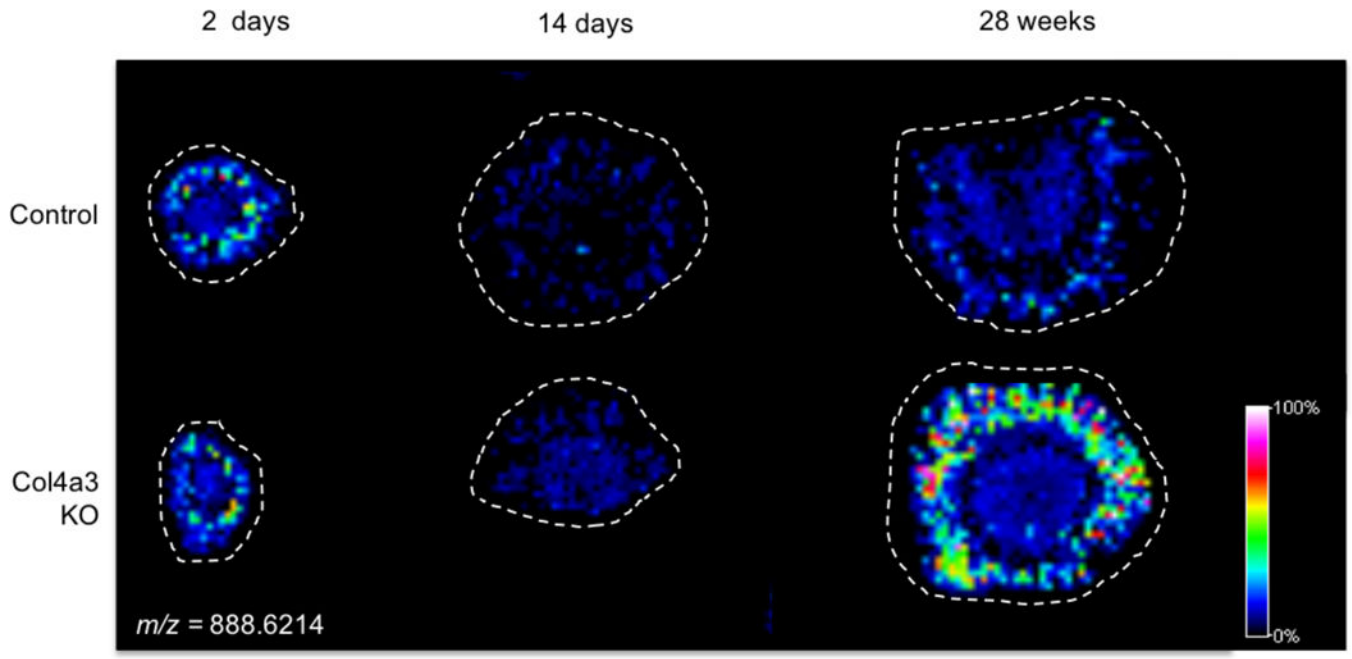

Fig. 1.

MALDI-IMS images of *m/z* 888.6214 in kidneys from wild-type and Alport mice generated by MALDI IMS analysis. Images were recorded in 2 day, 14 day, and 28 day-old mice from each group. The feature at *m/z* 888.6214 was identified as Sulfo-HexCer (18:3) and is re-expressed in the Alport mice only. Another Sulfo-Hex Cer, with *m/z* 776.5005 were nearly identical as the species were co-localized and were re-expressed in the Alport mice, only (not shown). Signal intensity is shown by a heat map as indicated by the scale bar. Kidney sections were cut transversely, to include tissue from both medulla and cortex.

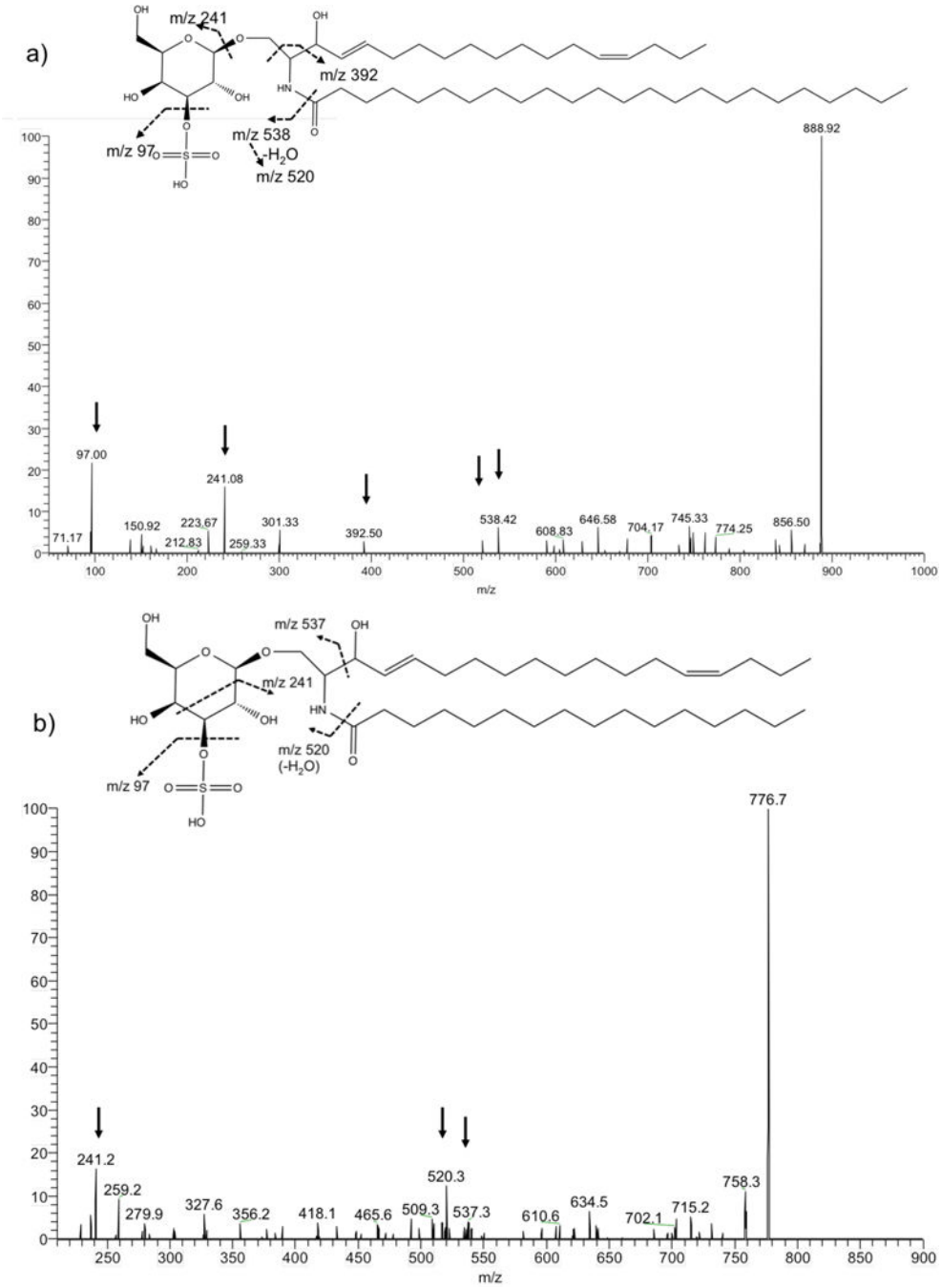

Fig. 2.

Chemical structures and MALDI MS/MS spectra of (A) Sulfo-HexCer (18:2, 24:0) and (B) Sulfo-HexCer (18:2, 16:0). These sulfo-HexCer lipids were found to be differently expressed in the Alport and WT mice. In the chemical structures, the double bonds in the sphingoid base are shown at their most common known positions, but these positions were not determined, experimentally. MALDI MS/MS data were collected using pulsed-q-dissociation and the spectra were recorded directly from the tissue surface. The spectra show features corresponding to the sulfo-sugar moiety (*m/z* 241, 259, 97) and the peaks

characteristic of the doubly saturated ceramide (*m/z* 538, 520, 392) (indicated in the spectra by arrows).

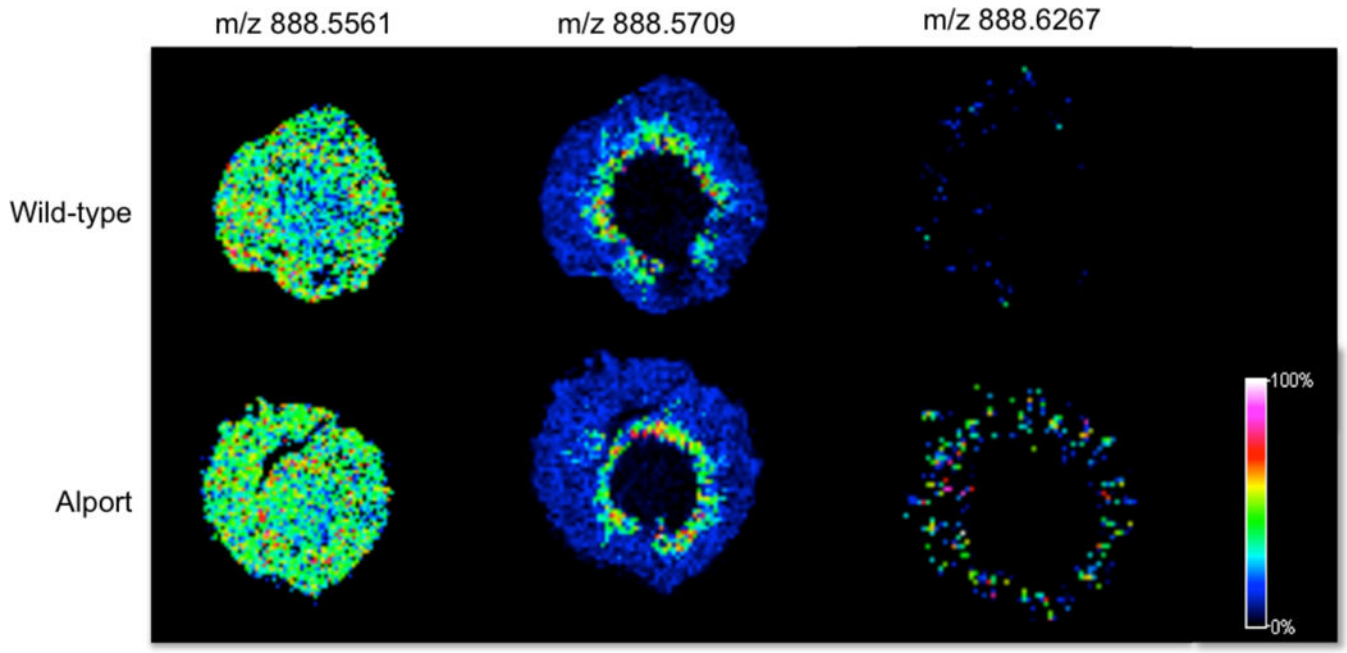

Fig. 3.

MALDI-IMS images of kidney sections from 28-day-old mice show the distribution and relative abudnace of ions with *m/z* 888.5561, 888.5709, and 888.6267. The abundance of each is indicated by a heatmap. Based on accurate mass, the peaks at *m/z* 888.5561 and 888.5709 correspond to C^{13} isotopes of phospholipids (PI(36:4) and PI(36:3), while *m/z* 888.6267 corresponds to the species of interest, i.e. SulfoHexCer(18:2/24:0). In contrast to the sulfatide, the two phospholipids were present at similar levels in the wild-type and Alport kidneys of 28-day old mice. High mass accuracy is necessary to separate near isobaric lipid species.

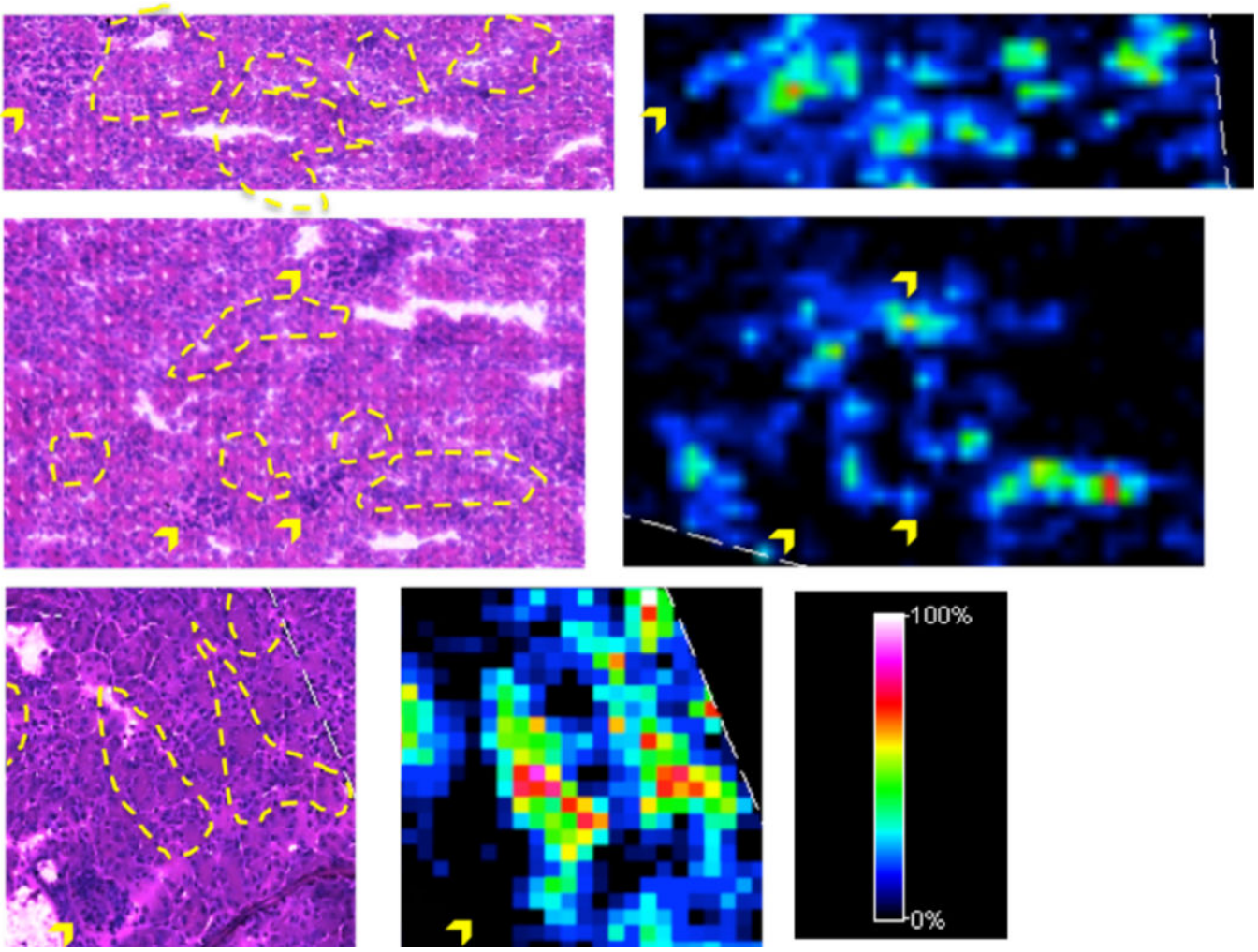

Fig. 4.

Examples of MALDI IMS images of *m/z* 888.6224 in the kidneys of 28-day old Alport mice recorded at 15 μm spatial resolution. The relative abundance of MS signals is indicated by a heat map. Tissue was stained using a PAS stain, after MS analysis and matrix removal. Areas corresponding to high MS signal are marked by a yellow dashed line in the stained tissue and the locations of glomeruli are indicated with yellow arrows. The raster pattern of the laser is apparent in the small arrays of damaged tissue. The signal appears to be colocalized to tubules and absent in glomeruli.